Design of a 50.000-r/min Synchronous Reluctance Machine for an Aeronautic Diesel Engine Compressor

Design of a 50.000 rpm Synchronous Reluctance Machine for an Aeronautic Diesel Engine Compressor

Marco Palmieri, Maurizio Perta, Francesco Cupertino
Department of Electrical Engineering and Information Technology
Politecnico di Bari
Bari, Italy
marcopalmieri.pm@gmail.com francesco.cupertino@poliba.it

***Abstract*—This paper describes the design procedure followed to realize a high-speed synchronous reluctance machine for aeronautical application. The attention is mainly focused on the rotor design that is the most critical part of any synchronous reluctance machine, in particular for high-speed applications. After a preliminary optimization of the rotor geometry, a multi-physical design that considered mechanical, thermal and electromagnetic properties was developed. The main steps of the design procedure together with an extensive analysis of the final design are presented here. Two prototypes have been realized using different rotor lamination materials in order to validate the design procedure.**

I. INTRODUCTION

High-speed AC electrical machines are gaining a remarkable interest in a wide range of application because they allow compact and high reliable solutions by eliminating mechanical gearboxes [1]-[4]. The actual trend in high speed electromechanical drives technology is focused on PM machines, solid rotor induction motors and switched reluctance motors [2],[5]. Very high rotational speeds, up to 500,000 rpm, have been recently reached by surface permanent magnet (PM) motors using retaining sleeves to ensure rotor integrity [6],[7]. A retaining sleeve has been also adopted for an 8kW 40,000 rpm internal permanent magnet (IPM) machine in [8]. Unfortunately, retaining sleeves may increase rotor losses and make rotor construction more complicated. In aeronautical applications, machine performances have to be guaranteed also in low-pressure environment. Then, the rotor cooling becomes a critical issue that could be faced using complicated shaft cooling systems and/or limiting rotor losses. Cage rotor induction machines and switched reluctance ones have an inherently robust rotor structure, suitable for high-speed applications. However, the former machines are characterized by higher rotor losses, the latter present higher torque ripple and both allow lower torque density when compared with PM machines [6]. Alternative solutions to avoid rotor sleeves could be also offered by solid rotor synchronous reluctance (SyR) machines [9], [10] but special manufacturing processes and special materials are needed to achieve satisfactory performances in terms of torque density and efficiency.

Transversally laminated multiple barriers SyR machines could constitute a viable and cheaper alternative for high-speed applications [11]. These machines, despite the reduced toque density (with respect to PM motors) or rotor robustness (with respect to solid rotor or switched reluctance ones), are easy to manufacture, require standard materials and allow good efficiency, high reliability and cost reduction [12]. As rotational speed increases, a multi-physics design approach becomes mandatory in order to take into account mechanical, thermal and electromagnetic issues and their mutual influence on machine overall performance [2], [5], [11]-[13]. In absence of a retaining sleeve, rotor integrity has to be guaranteed by tangential (near the airgap) and radial (in the middle of the barrier) ribs: thicker ribs increase the lamination robustness but, at the same time, reduce the saliency ratio of the machine, worsening torque and power factor figures [12], [14]. In this paper, a 5 kW – 50,000 rpm transversally laminated SyR machine is considered as case study to investigate the potentials of such technology in high-speed applications. The motor is designed so to realize an electrically-driven compressor for a two-strokes aeronautic diesel engine. The main steps of the design procedure together with an extensive sensitivity analysis of the final design are presented here. Two prototypes, having different rotor laminations materials were realized. The obtained results validate the design procedure and evidence the impact of lamination mechanical and magnetic properties on the SyR prototypes.

II. SPECIFICATIONS AND PRELIMINARY SIZING

The design of the SyR machine is based on specifications and considerations related to the considered final application. The most relevant are summarized in TABLE I. Due to the high-speed requirements (base speed equal to 50,000 rpm), the number of poles pairs is fixed to 2, in order to limit the fundamental frequency. A higher number of poles, in fact, would rapidly increase iron loss in the motor and commutation loss of the power converter. This is due to

the increased switching frequency needed to obtain reasonable current control performances in high-frequency applications. Machine overall axial length and external diameter are fixed by the maximum available volume, while a minimum shaft diameter and airgap thickness are imposed by mechanical constraints. The motor is supposed to be liquid cooled using the engine fuel flowing through a spiral coil around the stator laminations. The maximum current density in stator windings is determined after a thermal analysis by means of a lumped-parameters equivalent thermal model of the machine. The absence of a dedicated cooling system for the rotor suggested guiding the design towards the reduction of rotor losses.

TABLE I – MACHINE SPECIFICATIONS

Parameter	Value	Units
Rated speed	50000	Rpm
Rated Power	5	kW
Rated DC bus voltage	270	Vdc
Overload torque (60 s)	1.6	Nm
Pole pairs	2	--
Current density	<20	Arms/mm2
Slot filling factor	<0.4	--
Shaft Diameter	13	mm
Maximum copper temperature	140	°C
Inlet liquid cooling temperature	20	°C
Liquid cooling flow-rate	5	l/min
Outer diameter	90	mm
Axial length	130	mm

Following the guidelines reported in [15], a special care is paid for the selection of lamination materials: with the aim of improving torque density and efficiency, a cobalt-iron (CoFe) alloy with high flux density and low losses is selected for stator lamination. The prototype is realized using *Vacodur 49* from Vacuumschmelze [16] with thickness of laminations equal to 0.15 mm. Stator laminations are wire cut and heat-treated so to enhance electromagnetic properties (saturation flux density over 2 T). As regards the rotor, it was initially designed considering the same CoFe alloy used for the stator, but differently annealed in order to maximize structural properties (Yield strength equal to 390 MPa). Then, to increase the safety factor on rotor stress and obtain an infinite expected life after fatigue analysis, the same rotor geometry was also realized using the 10JNEX900 from JFE-steel corporation [17]. This is a SiFe alloy with a lamination thickness of 0.1 mm, enhanced mechanical properties (Yield strength above 600 MPa) and lower losses due to the high silicon content. This will allow to compare the impact on SyR performances of both mechanical and magnetic steel properties. Figure 1 shows the BH curves for the considered materials, while Table II summarizes their main properties.

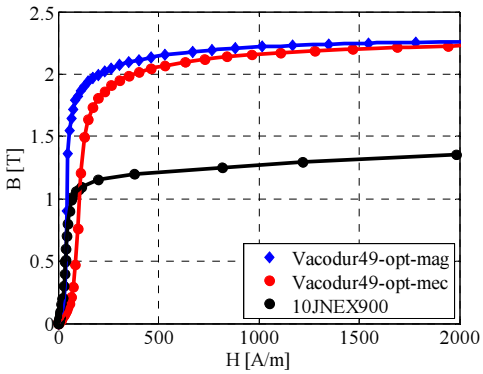

Figure 1- BH characteristics of the considered alloys

TABLE II– ELECTRICAL AND MECHANICAL PROPERTIES OF IRON ALLOYS

Lamination Type	Vacodur opt-mag	Vacodur opt-mec	JNEX900
Loss @ 50 Hz, 1.5 T [W/kg]	1.27	2.78	1.46*
Loss @ 400 Hz, 1.5 T [W/kg]	14.7	26.4	14.8*
Yield strength [MPa]	210	390	604
Mass density [kg/m^3]	8120	8120	7490

* Extrapolated values

III. DESIGN PROCEDURE

A. *Preliminary electromagnetic design*

Regarding rotor geometry, the parameters that mostly affect the average torque and its ripple are the flux barrier number and thickness and the position of rotor slots (barrier ends) at the airgap. It was already demonstrated that a simplified flux barrier geometry, described by a reduced number of parameters, can guarantee the same performances of more complex geometries but is better suited for automated design assisted by optimization algorithms [18], [19]. After a trade-off analysis, the final choice for this project was to use a rotor with an outer straight flux barrier (having the shape of I) and inner flux barriers each made of three straight segments (similar to the shape of a U). Such geometry fits also well with the insertion of sintered magnet in the flux barriers in order to improve power factor and realize a PM-assisted synchronous reluctance machine [20], [21]. Even if this possibility could be exploited for future researches, the attention of this study is only focused on machines without permanent magnets.

A preliminary investigation was carried out using finite element analysis and optimization algorithms to select the most appropriate number of stator and rotor slots. Stators having 12, 24 and 36 slots with distributed windings and rotors with a number of barriers per pole variable from 1 to 5 were considered [22]. Generally, solutions with a lower stator and rotor slot number tend to have poor performances in terms of average torque and torque ripple. On the other hand, performances improve with higher slots number, but the practical realization of the machine could become complicated in case of small high-speed motors. Moreover,

for a given stator, the higher the number of rotor slots, the higher the rotor iron losses. Since the reduction of rotor losses is a primary concern, due to the absence of a dedicated rotor cooling system, the adoption of high stator and rotor slot number is discouraged. A machine having 24 stator slots (12 slots per pole pair) and three rotor barriers per pole is selected as the best compromise between electromagnetic performances and feasibility of the prototype. An electromagnetic optimization of the rotor geometry was performed according to the guidelines reported in [18] and [19]. Average torque and torque ripple, FEA-evaluated, were considered as objective functions, while the barriers' thicknesses and their angular displacements at the airgap were chosen as optimization parameters. For sake of computational speed, the optimization procedure was performed at a single current value; moreover the current phase angle in the dq-reference frame was included among the optimization parameters in order to fast evaluate the maximum torque per ampere condition without further simulations. The effectiveness of such design procedure was experimentally proven in [23]. The rotor selected after this stage is shown in Figure 2.

B. *Optimization of rotor ribs*

In order to simplify as much as possible the realization of the machine so to fully exploit the advantages of a SyR machine for high-speed applications, it was decided to avoid any retaining sleeve and rely only on rotor ribs to withstand centrifugal forces and guarantee rotor integrity. The preliminary design shown in Figure 3a, having only tangential ribs, was too weak to withstand the centrifugal forces at 50,000 rpm. Radial ribs were added to the inner flux barriers and their number, position and thickness were designed with the aid of an optimization algorithm. The position at airgap and thickness of the flux barriers was kept constant during ribs optimization. The optimization procedure returned a number of different rotors with similar mechanical strength properties [13]. Their electromagnetic properties (torque, power factor, losses) were all evaluated so to select the best compromise machine, which is shown in Figure 3b. The mechanical optimization was performed considering a stress limit below 390 MPa so to allow the use of both CoFe and SiFe alloys.

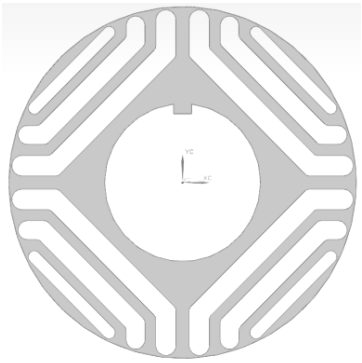

Figure 2 – Preliminary rotor design

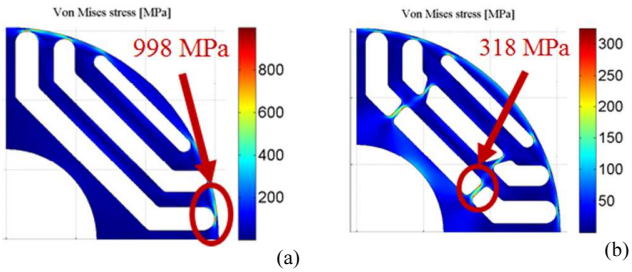

Figure 3 – Stress distribution (MPa) evaluated by means of structural FEA on preliminary (a) and final (b) rotor

IV. SENSITIVITY ANALYSIS

A sensitivity analysis wass carried out on the final design in order to evaluate the impact of geometric variations on motor performance.

A. *Airgap thickness variation*

The airgap thickness has a strong impact on magnetic performance since it is strictly related to the d-axis reluctance (see Figure 5). Figure 4 reports some selected results obtained changing the airgap value in the range from 0.1 to 0.4 mm. When the airgap is reduced there is an increase of both average torque and power factor when stator current amplitude is kept constant. On the other hand, a thicker airgap produces a filtering effect on torque harmonics, thus reducing the torque ripple. Mechanical constraints regarding rotor deformation and thermal expansion, together with practical issues related to manufacturing tolerances, impose a lower limit for the airgap thickness. After some calculations about the dynamic deformation of the rotor structure, a conservative airgap value equal to 0.25 mm was selected for the first prototype. A less conservative choice could allow to approach a power factor value closer to 0.7 that can be considered as the maximum feasible value for the considered machine topology in such application.

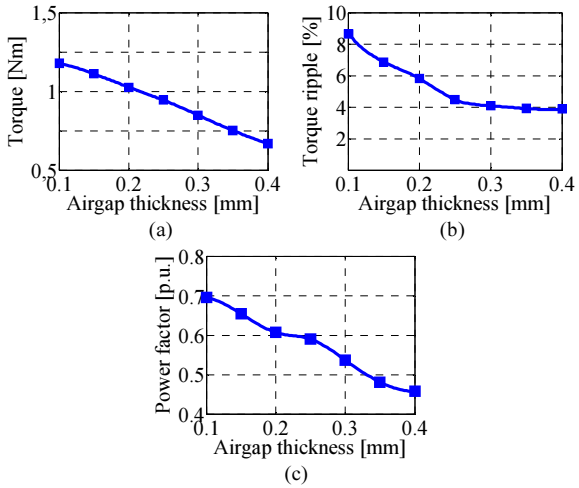

Figure 4 - Average torque (a), torque ripple (b), and power factor (c) at constant stator current amplitude as a function of airgap

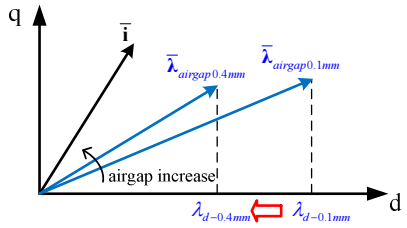

Figure 5 - Vector diagram of flux linkage variation with airgap thickness

B. *Rotor ribs variation*

Tangential and radial ribs have a strong influence on SyR machines performance, as explained in the previous section. From a structural standpoint, they are unavoidable in order to ensure rotor integrity against centrifugal forces; but from electromagnetic point of view (see Figure 7) they produce flux increase across the high reluctance q-axis of the machine, thus deteriorating average torque and power factor. Figure 6 shows the impact of manufacturing tolerances comparing the designed machine *M* with two machines, namely *T*- and *T*+, having ribs thickness respectively decreased (minus 0.05 mm) and increased (plus 0.05 mm) so to account for minimum and maximum tolerances of the cutting process.

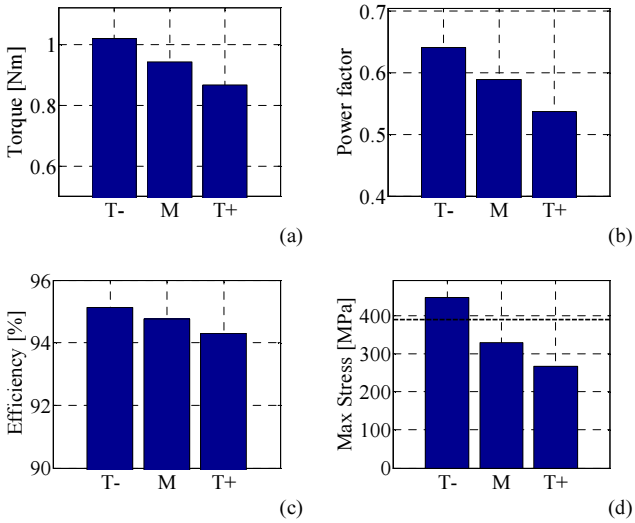

Figure 6 - Average torque (a), power factor (b), efficiency (c) and maximum stress (d) at constant current amplitude as a function of iron ribs

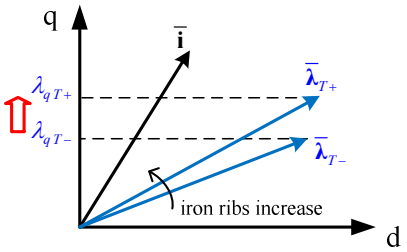

Figure 7 – Vector diagram of flux linkage variation with iron ribs thickness

C. *Shaft radius variation*

The shaft diameter is strictly related to mechanical performance and it has to be evaluated considering rotor-dynamic issues in addition to maximum torque and speed requirements [5],[24]. However, these aspects exceed the scope of this paper. At this stage, the influence of shaft radius on the maximum stress due to centrifugal forces is evaluated by means of structural finite element analysis (FEA). As shown in Figure 8, a thicker shaft increases the maximum stress because of the reduced amount of iron mass between the shaft and the inner barrier; the maximum stress is always located near the radial ribs of the inner U-shaped barrier.

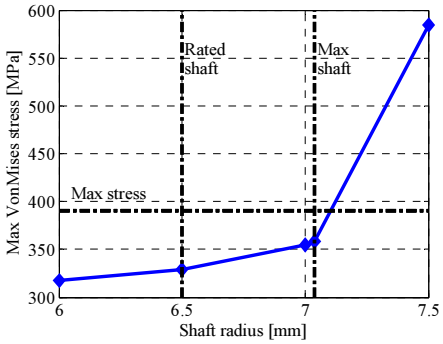

Figure 8 - Maximum stress as a function of shaft radius

When the iron between shaft and inner barrier becomes too thin, the maximum stress value rapidly reaches unacceptable values. This analysis allowed to determine a maximum shaft radius equal to 7.04 mm, as highlighted in Figure 8. It was verified that shaft diameter variations, below the mentioned limit, have negligible effects on electromagnetic performance.

D. *AC copper losses analysis*

In order to evaluate the impact of AC additional copper losses due to proximity effect, some investigations were carried out using both finite element analysis and experimental tests on stator prototypes. For sake of brevity the results shown here (Figure 10) are limited to two different winding configurations. Both of them use a bundle of 12 parallel strands each with diameter equal to 0.31 mm. One winding is made of traditional random wound coils; the other one is realized adding a 180 degrees rotation at the bundle along each active side of the coil. The obtained copper filling factor is equal to 0.39 in both cases. The increase of coils length due to the single twisting along each active side of the coil is negligible. Twisting allowed a reduction of additional AC losses from 24% to 12% of DC losses at motor rated frequency, as demonstrated by experimental results reported in Figure 10. This is a good achievement considering that the winding are realized using a manual winding machine and manually inserted in the slots wire by wire. Twisting multiple times the coils along each active side of the stator, or introducing Litz-type wires, would further decrease the AC losses but also compromise

the performances at lower frequency due to the increased coils length and decreased filling factor.

Different stator winding chording are also studied. Due to chosen numbers of poles and stator slots, all the windings have 2 slots per pole per phase, thus three possible coils arrangements were considered: W0 (not chorded), W1 (1 step) and V2 (2 steps). Rotor iron losses decrease with winding chording, but the reduction of the average torque value is even more important, as demonstrated by the decreasing values of motor efficiency (see Figure 9). Not chorded winding was finally selected because it simplifies the stator manufacturing and allows a better copper filling factor.

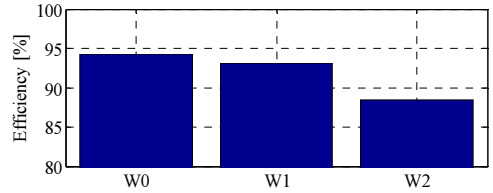

Figure 9 – Efficiency at rated current and speed as a function of winding chording

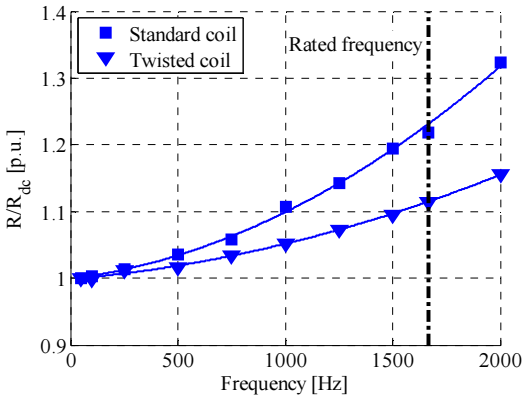

Figure 10 - R/R_{dc} ratio versus frequency using different coil configurations (blue and red squares are measured values)

V. Analysis of the Final Design

Table III reports the main geometrical parameters of the machine laminations, while Table IV summarizes their performance. Two prototypes differing only for the rotor lamination material are analyzed. Figure 11 - Figure 14 report some contour plots in the id-iq plane for the CoFe rotor (left columns) and SiFe rotor (right column); the rated current loci, which are slightly different for the two machines, are highlighted by dashed line. Due to different magnetic properties, the motor with SiFe rotor requires a current value 9% higher than CoFe one to produce similar torque values.

In particular, Figure 11 evidences average torque loci; torque ripple, calculated as the standard deviation of the torque over an electrical period, is about 4.7% at rated current and below 5% also at 150% rated current in the worst case (Figure 12). Moreover the SiFe machine shows reduced torque oscillations due to the different magnetic behavior of the SiFe alloy.

Figure 13 focuses on power factor loci: at rated current and near the Maximum Torque Per Ampere (MTPA) phase angle, it is quite low. This is one of the major drawbacks of SyR machines, which could be partially overcome by a less conservative airgap value, as reported in Section IVa. Moreover, a further solution to improve power factor is the insertion of a small amount of PMs within the rotor barriers so to have a PM-assisted SyR machine [20]. Such solution is deeply investigated in [21].

Figure 14 shows the overall efficiency calculated at 50,000 rpm (which is the rated motor speed). Rotor losses of SiFe are negligible when compared to CoFe ones; moreover they are limited under 50 W for both machines and efficiency is always above 94 % in the load range from 100% to 150% of rated torque.

TABLE III - GEOMETRIC PARAMETERS OF MACHINE LAMINATIONS

PARAMETER	VALUE	UNITS
STATOR EXTERNAL RADIUS	26.20	mm
ROTOR RADIUS	15.25	mm
AIR GAP	0.25	mm
SHAFT RADIUS	6.5	mm
ROTOR RIBS	0.20 - 0.30	mm
AXIAL LENGTH	50.00	mm

TABLE IV - MACHINE PERFORMANCE

PARAMETER	COFE ROTOR	SIFE ROTOR	UNITS
RATED TORQUE	0.96	0.96	Nm
RATED CURRENT	33.2	36.2	A_{rms}
CURRENT DENSITY	18	20	A_{rms}/mm^2
TORQUE RIPPLE AT RATED CURRENT	4.3	2.85	%
MAX POWER FACTOR	0.61	0.62	--
COPPER LOSS AT 50,000 RPM	151	179	W
STATOR IRON LOSS AT 50,000 RPM	89	79	W
ROTOR IRON LOSS AT 50,000 RPM	46	9	W

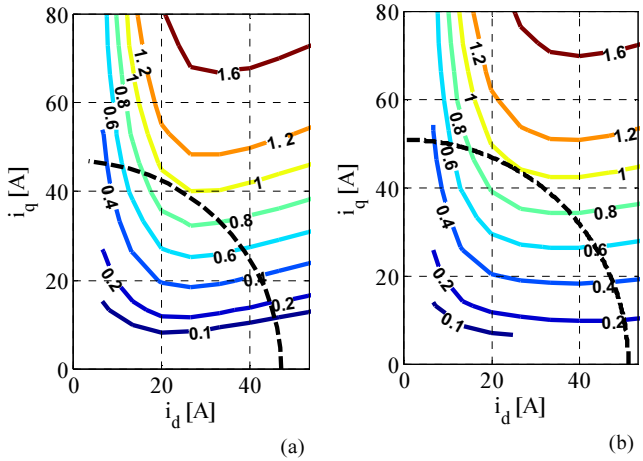

Figure 11 – Contour plots of mean torque for CoFe (a) and SiFe (b) rotors

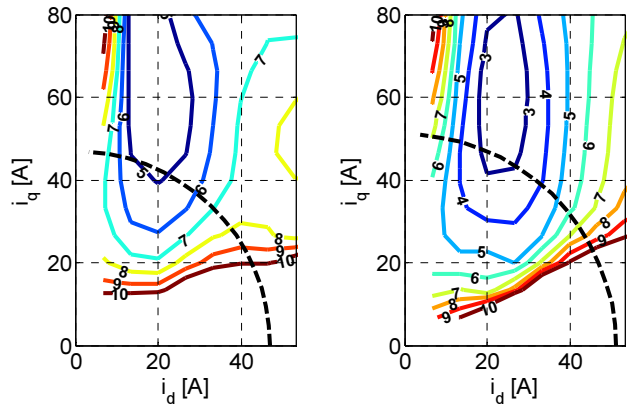

(a) (b)

Figure 12: Contour plots of torque ripple for CoFe (a) and SiFe (b) rotors

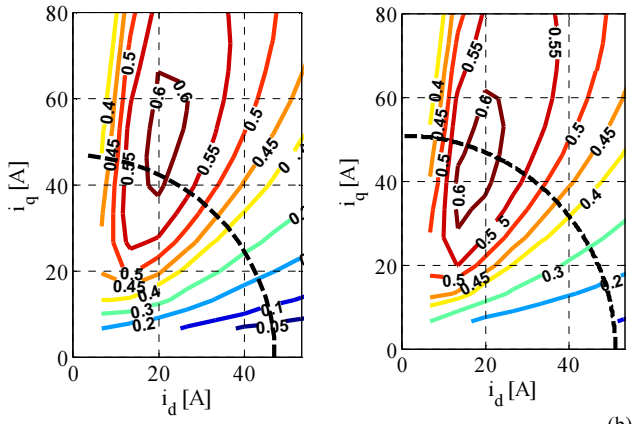

(a) (b)

Figure 13 - Contour plots of power factor for CoFe (a) and SiFe (b) rotors

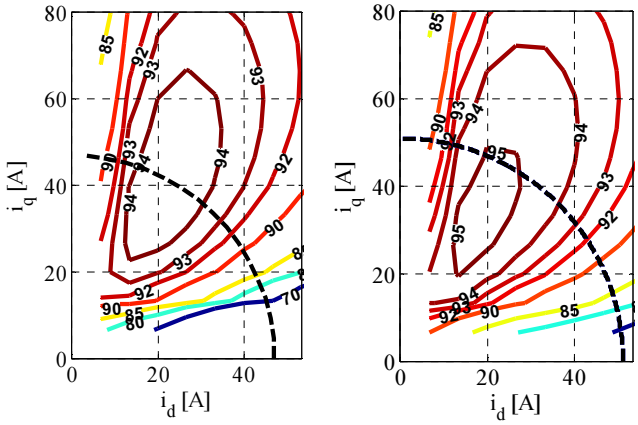

(a) (b)

Figure 14 - Contour plots of efficiency at 50,000 rpm for CoFe (a) and SiFe (b) rotors

From the abovementioned analysis it is clear that, at high-speed regimes, the lower losses steel grade allows an efficiency increase despite the lower saturation level. A moderate advantage in terms of power factor also allows to reduce power converter sizing.

VI. Experimental Results

Two prototypes ,were realized. Both SyR machines share the same geometrical dimensions and stator material (i.e. CoFe alloy Vacodur49-opt-mag) while they differ for the rotor lamination alloys: for the first rotor is adopted the CoFe Vacodur49-opt-mag; the second rotor is realized using the SiFe 10JNEX900. All the CoFe laminations were wire-cut, whereas the SiFe rotor was laser-cut; for both rotors, the tolerances declared by the manufacturers were equal to 0.04 mm for the rotor external circumference and 0.05 mm for the flux barriers profiles. Due to the small geometrical dimensions of rotor laminations (see Table III), no additional machining was performed after the cutting process.

Both machines are equipped with precision high-speed bearings; in particular, sealed bearings with steel balls (supplied already greased using high speed lubricant) were adopted since they can reach up to 67,000 rpm.

The prototypes were tested on a dedicated test bench that includes a torque meter, a 20kHz back-to-back IGBT converter supplied via a DC power supply and a dSPACE 1006 board used to implement vector control on both machines (see Figure 15). Figure 16 shows the test bench together with stator and rotor laminations before machine assembly. The two machines are mechanically coupled and alternatively speed-controlled and torque-controlled during the magnetic model identification procedure. Further details about the experimental magnetic model identification can be found in [25]. The d- and q- axis current responses after a step change of the set-point are reported in Figure 17. The bandwidth of the current controllers is close to 500Hz. The current responses are fast and over-damped with a limited ripple despite the low inductance values. Since the specific application does not require very fast dynamic responses the focus of the current controller setting is the control stability at high-speed regimes more than the torque step response. Figure 18 illustrates the result of a no-load speed acceleration from zero to 50,000 rpm. These results confirm the good dynamic properties of the control system and the low value of the friction torque even at high speed. More details about the current controller tuning are reported in [26].

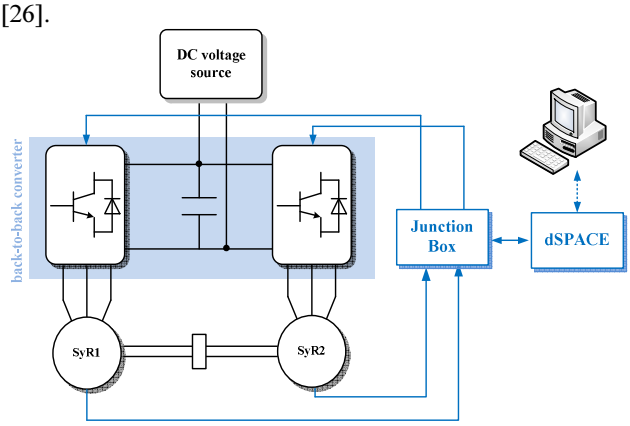

Figure 15 – Block diagram of the test bench

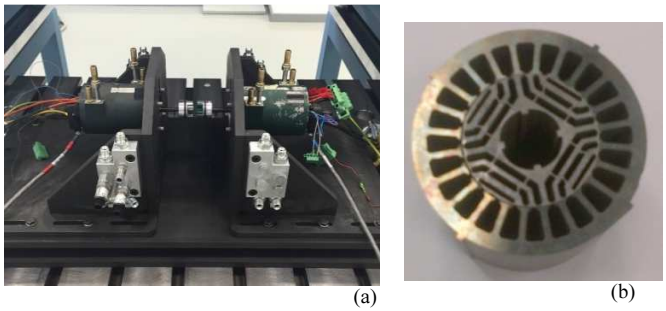

(a) (b)

Figure 16 – Experimental test bench (a), top-view of lamination stacks (b)

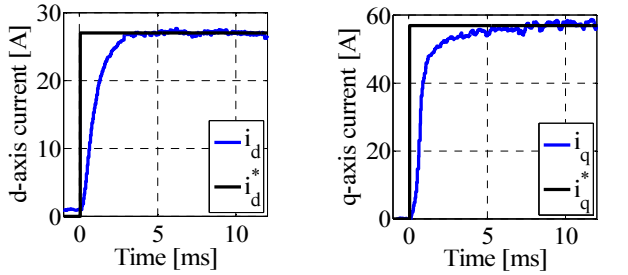

(a) (b)

Figure 17 - Exp results: step change of d-axis (a) and q-axis (b) currents

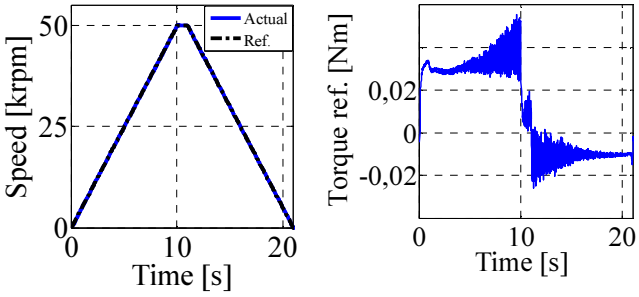

(a) (b)

Figure 18 – Experimental results: mechanical speed responses up to rated speed at no-load

FEA simulations and experimental results were compared for the two machines. For sake of brevity the results obtained at few current values in the region of practical interest, are presented in Table V. Moreover, the last column of Table V shows FEA results obtained considering the worst-case condition (i.e. maximum increase of rotor ribs and airgap radius within the limits of mechanical tolerances) due to manufacturing process.

The differences between FEA and experimental flux modules approximate 10% and 2% for CoFe and SiFe rotors respectively if manufacturing tolerances are neglected. This leads to a quite large gap between simulated and measured torque, since the d-axis flux is overestimated while the q-axis one is underestimated for both the rotor materials (see Figure 19). Conversely, by taking into account the manufacturing tolerances (dashed vector in Figure 19), the FEA simulation results match well with experimental ones as reported in the last two columns of Table V. In this case, the maximum error between simulations and experiments is less than 8% for average torque in the worst case.

Moreover the torque ripple, measured by mechanically locking the rotor in different positions, is 6% when rated current amplitude and MTPA phase angle are considered; these results are in good agreement with the values reported in the previous section.

TABLE V – COMPARISON BETWEEN FEA AND EXPERIMENTAL VALUES

ROTOR	TEST	SIM	EXP	SIM$_T$
CoFe	Id =24A	λ_d =11.9mWb	λ_d =10.0mWb	λ_d =9.9mWb
	Iq =36A	λ_q =5.0mWb	λ_q =6.3mWb	λ_q =5.7mWb
	Id =24A	λ_d =12.1mWb	λ_d =10.2mWb	λ_d =10.0mWb
	Iq =30A	λ_q =4.5mWb	λ_q =5.6mWb	λ_q =5.2mWb
	Id =18A	λ_d =9.9mWb	λ_d =7.9mWb	λ_d =7.6mWb
	Iq =36A	λ_q =5.2mWb	λ_q =6.5mWb	λ_q =5.8mWb
SiFe	Id =24A	λ_d =9.8mWb	λ_d =9.1mWb	λ_d =8.8mWb
	Iq =36A	λ_q =4.1mWb	λ_q =5.7mWb	λ_q =4.7mWb
	Id =24A	λ_d =9.9mWb	λ_d =9.3mWb	λ_d =8.9mWb
	Iq =30A	λ_q =3.6mWb	λ_q =5.1mWb	λ_q =4.3mWb
	Id =18A	λ_d =8.0mWb	λ_d =7.1mWb	λ_d =7.0mWb
	Iq =36A	λ_q =4.2mWb	λ_q =5.8mWb	λ_q =4.8mWb

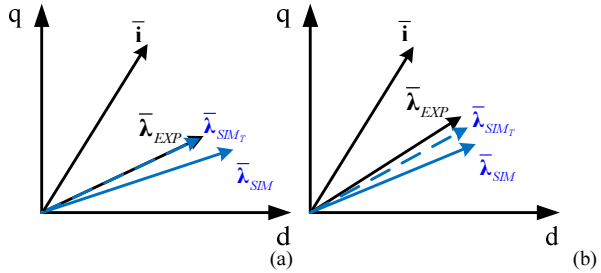

(a) (b)

Figure 19 – Comparison of simulated and experimental fluxes for CoFe (a) and SiFe (b) rotor machines

Several tests were also performed to check the effectiveness of the cooling system. Figure 20 reports some results obtained increasing the torque reference until the steady state copper temperature reached 140°C. The total losses in such condition are about 340 W, well above the motor losses at rated speed and torque that are less than 300 W for both the prototypes (see Table III).

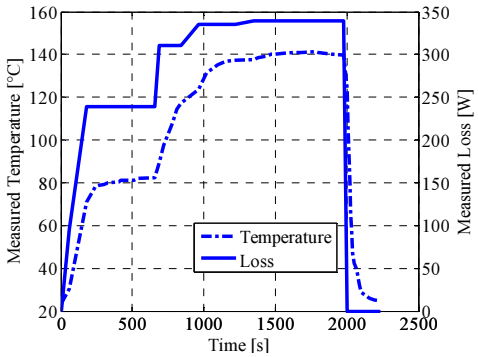

Figure 20 – Experimental results: total loss (solid line) and copper temperature (dashed line) measured during a warm-up and cooling test

VII. CONCLUSIONS

This paper presented the design procedure followed to realize a 50,000 rpm synchronous reluctance motor to be used coupled to a compressor for an aeronautical diesel engine. One of the key aspects of the presented design it the adoption of a rotor geometry with multiple flux barriers and non-oriented laminations as usual in low-speed applications, without a sleeve or any additional retaining structure. This choice greatly simplifies the rotor structure and its feasibility. Aim of the research was to investigate the performance limits of this kind of machine in high-speed applications. A prototype of the proposed motor was also realized and presented to validate the feasibility of the proposed high-speed motor.

ACKNOWLEDGMENT

The authors would like to thank dr. Alessandra Guagnano for her essential help in the test bench setup and experiments. This work was supported in part by project PON MALET – code PON01_01693.

REFERENCES

[1] D. Gerada, A. Mebarki, N.L. Brown, C. Gerada, A. Cavagnino, A. Boglietti, “High-Speed Electrical Machines: Technologies, Trends, and Developments”, IEEE Transactions on Industrial Electronics, Vol. 61, n. 6, 2014, pp. 2946-2959

[2] Moghaddam, R.R., "High speed operation of electrical machines, a review on technology, benefits and challenges," in Energy Conversion Congress and Exposition (ECCE), 2014 IEEE , vol., no., pp.5539-5546, 14-18 Sept. 2014

[3] Bartolo, J.B.; He Zhang; Gerada, D.; De Lillo, L.; Gerada, C., "High speed electrical generators, application, materials and design," Electrical Machines Design Control and Diagnosis (WEMDCD), 2013 IEEE Workshop on , vol., no., pp.47,59, 11-12 March 2013

[4] Hofmann H., Sanders S.R., “High-speed synchronous reluctance machine with minimized rotor losses”, IEEE Transactions on Industry Applications, Vol. 36, n. 2, 2000, pp. 531-539

[5] Gieras, J.F., "Design of permanent magnet brushless motors for high speed applications," Electrical Machines and Systems (ICEMS), 2014 17th International Conference on , vol., no., pp.1,16, 22-25 Oct. 2014

[6] Gerada D., Borg-Bartolo D., Mebarki A., Micallef C., Brown N.L., Gerada C., “Electrical machines for high speed applications with a wide constant-power region requirement”, International Conference on Electrical Machines and Systems, ICEMS 2011.

[7] Krahenbuhl D., Zwyssig C., Weser H., Kolar J.W., “A Miniature 500 000-r/min Electrically Driven Turbocompressor”, IEEE Transactions on Industry Applications, Vol. 46, n. 6, 2010, pp. 2459-2466.

[8] Sung-Il Kim ,Young-Kyoun Kim, Geun-Ho Lee, Jung-Pyo Hong, “A Novel Rotor Configuration and Experimental Verification of Interior PM Synchronous Motor for High-Speed Applications”, IEEE Transactions on Magnetics, Vol. 48, n. 2, 2012, pp. 843-846.

[9] Jae-Do Park, Kalev C., Hofmann H.F., “Analysis and Reduction of Time Harmonic Rotor Loss in Solid-Rotor Synchronous Reluctance Drive”, IEEE Transactions on Power Electronics, Vol. 23, n. 2, 2008, pp. 985-992

[10] Ikaheimo J., Kolehmainen J., Kansakangas T., Kivela V., Moghaddam R.R., “Synchronous High-Speed Reluctance Machine With Novel Rotor Construction”, IEEE Transactions on Industrial Electronics, Vol. 61, n. 6, 2014, pp. 2969-2975.

[11] Palmieri, M.; Perta, M.; Cupertino, F., "Design of a 50.000 rpm synchronous reluctance machine for an aeronautic diesel engine compressor," in Energy Conversion Congress and Exposition (ECCE), 2014 IEEE , vol., no., pp.5138-5143, 14-18 Sept. 2014

[12] Taghavi, S.; Pillay, P., "A comparative study of synchronous reluctance machine performance with different pole numbers for automotive applications," Industrial Electronics Society, IECON 2014 - 40th Annual Conference of the IEEE , vol., no., pp.3812,3818, Oct. 29 2014-Nov. 1 2014

[13] Di Nardo, M.; Galea, M.; Gerada, C.; Palmieri, M.; Cupertino, F., "Multi-physics Optimization Strategies for High Speed Synchronous Reluctance Machines," in Proceedings of Energy Conversion Congress and Exposition (ECCE), 2015 IEEE

[14] T. A. Lipo, T. J. E. Miller, A. Vagati, I. Boldea, L. Malesani, and T. Fukao, “Synchronous reluctance drives,” in Conf. Rec. IEEE IAS Annu. Meeting, Denver, CO, Oct. 1994

[15] Palmieri, M.; Perta, M.; Cupertino, F.; Pellegrino, G., "High-speed scalability of synchronous reluctance machines considering different lamination materials," in Industrial Electronics Society, IECON 2014 - 40th Annual Conference of the IEEE , vol., no., pp.614-620, Oct. 29 2014-Nov. 1 2014

[16] http://www.vacuumschmelze.com/

[17] http://www.jfe-steel.co.jp/en/

[18] Pellegrino G., Cupertino F.; Gerada C., “Barriers shapes and minimum set of rotor parameters in the automated design of Synchronous Reluctance machines” IEEE International Electric Machines & Drives Conference (IEMDC), pp. 1204-1210, 2013.

[19] Cupertino, F.; Pellegrino, G.; Gerada, C., "Design of Synchronous Reluctance Motors With Multiobjective Optimization Algorithms," in Industry Applications, IEEE Transactions on , vol.50, no.6, pp.3617-3627, Nov.-Dec. 2014.

[20] A. Fratta, A. Vagati, and F. Villata, “Design criteria of an IPM machine suitable for field-weakened operation,” in Proc. ICEM’90, 1990, pp. 1059–1065.

[21] Cupertino, F.; Palmieri, M.; Pellegrino, G., "Design of High Speed Synchronous Reluctance Machines," in Proceedings of Energy Conversion Congress and Exposition (ECCE), 2015 IEEE

[22] Palmieri, M.; Perta, M.; Cupertino, F.; Pellegrino, G., "Effect of the numbers of slots and barriers on the optimal design of synchronous reluctance machines," in Journal of Electrical Engineering, Politehnica Publishing House, Vol. 15, no. 1, pp. 325-333, January 2015.

[23] Pellegrino, G.; Cupertino, F.; Gerada, C., "Automatic Design of Synchronous Reluctance Motors Focusing on Barrier Shape Optimization," in Industry Applications, IEEE Transactions on , vol.51, no.2, pp.1465-1474, March-April 2015

[24] Rao J.S.: Rotor Dynamics, 3rd ed. New Delhi: New Age Int Publishers, 1983

[25] Armando, E.; Bojoi, R.I.; Guglielmi, P.; Pellegrino, G.; Pastorelli, M., "Experimental Identification of the Magnetic Model of Synchronous Machines," in Industry Applications, IEEE Transactions on , vol.49, no.5, pp.2116-2125, Sept.-Oct. 2013

[26] Altomare, A.; Guagnano, A.; Cupertino, F.; Naso, D., "Discrete-time control of high-speed salient machines," in Industry Applications, IEEE Transactions on , vol.52, no.1, pp.293-301, Jan.-Feb. 2016.